A fundamental shift in the melt processes of Arctic sea ice

Jeremy Wilkinson (jpw28@bas.ac.uk)
British Antarctic Survey
Martin Doble
Polar Scientific Ltd
Lovro Valcic
Bruncin
Gaelle Veyssiere
British Antarctic Survey
Sylvia Cole
Woods Hole Oceanographic Institution
Luc Rainville
Applied Physics Laboratory, University of Washington
Craig Lee
Applied Physics Laboratory, University of Washington
John Hargrove
Center for Southeastern Tropical Advanced Remote Sensing, University of Miami
Julia DiLeo
Center for Southeastern Tropical Advanced Remote Sensing, University of Miami
Hans Graber
Center for Southeastern Tropical Advanced Remote Sensing, University of Miami

Article

Keywords: Arctic sea ice, melt cycle, marine ecosystem

Posted Date: September 8th, 2020

DOI: https://doi.org/10.21203/rs.3.rs-63411/v1

A fundamental shift in the melt processes of Arctic sea ice

Jeremy Wilkinson [1*], Martin Doble[2], Lovro Valcic[3], Gaelle Veyssiere[1], Sylvia T. Cole[4], Luc Rainville[5], Craig Lee[5], John Hargrove[6], Julia DiLeo[6], Hans Graber[6]

Affiliations:

[1*] British Antarctic Survey, Cambridge, UK.

[2] Polar Scientific Ltd, Appin, Scotland, UK.

[3] Bruncin, Zagreb, Croatia.

[4] Woods Hole Oceanographic Institution, Woods Hole, USA.

[5] Applied Physics Laboratory, University of Washington, Seattle, USA.

[6] Center for Southeastern Tropical Advanced Remote Sensing, University of Miami, Miami, USA.

As the Arctic Ocean transitions into a seasonally ice-covered ocean, the processes that govern the sea ice melt cycle will undergo a fundamental shift. The summer melt cycle passes through several stages, such as snowmelt, meltpond formation and drainage, and basal melting; normally with surface melt processes occurring well before basal melt. Monitoring of atmospheric, sea ice and oceanographic properties from autonomous buoys deployed across the Beaufort Sea, combined with targeted satellite imagery, reveal a fundamental restructuring of these melt processes within the seasonal ice zone – where basal melt occurs before surface melt. We find this seemingly unremarkable change accelerates the basal melting of sea ice by ten-fold, as well as transforming the timing and flux of freshwater and heat into the upper-ocean. These processes play a pivotal role in determining upper-ocean stratification, and when combined with a modification of the under-ice light field, it could impact marine ecosystem function.

Arctic sea ice is a key climate indicator and many of its properties have been monitored for decades, during which time we have observed changes in many aspects of its lifecycle. From a decline in sea ice extent in all seasons *(1)*, to a reduction in its

thickness *(2)*, a decline in multiyear ice and its replacement by first-year ice *(3)* and variations in its drift *(4)*. In summer, these changes have led to the sea ice edge retreating further northwards, and a more fractured state for the sea ice that remains *(5)*. These changes are consistent with an Arctic Ocean transitioning from a perennial sea-ice cover to a seasonal ice regime *(6)*. The Beaufort Sea epitomizes this transition as it now has a predominately seasonal ice cover, and in the spring and summer large expanses of the Beaufort are subject to low concentrations of sea ice, or even ice-free conditions in its southernmost regions.

Ice-albedo feedback is regarded as the most important mechanism controlling surface and basal melt processes *(7)*. The basis of this is the stark contrast in albedo between the snow on the sea ice (> 0.8, see *(8)*) and that of open-water (~0.07, see *(9)*). Surface melt transitions through three broad stages *(10)*. During Stage 1 the snow melts and the meltwater spreads out over the surface forming large lakes, because the ice is initially impermeable to meltwater. Stage 2 is characterised by the rapid drainage of these lakes, via the opening of macroscopic flaws in the ice, reducing the size and area covered by meltponds. Stage 3 involves processes such as surface ablation and meltpond evolution that occur late in the season, and are beyond the scope of this study.

Basal melt occurs through a different process. As the season advances the ice pack weakens, becomes more divergent and fractured, producing larger areas of open water. Because of the very low albedo of the ocean surface it preferentially absorbs solar radiation, warming the upper-ocean. Once the ocean temperature rises above its freezing-point basal melting begins *(11*), which provides a near-constant freshwater flux (until the ice is completely melted).

Traditionally the Arctic Ocean in summer consisted of high ice concentrations of perennial ice, with only the peripheries experiencing short periods of lower ice concentration or open-water. With limited breakup and divergence sea ice melt was predominately controlled by surface melt processes, with a lesser amount being basal melt *(12)*. However, the Arctic Ocean is presently transitioning towards a seasonal ice cover, and understanding how this influences the timing of surface and basal melt processes and its impact on the upper-ocean is a priority *(13-14)*.

1. Data

In Autumn 2018, several autonomous buoys were deployed on the sea ice within the northern regions of the Beaufort Sea. These systems monitored key atmospheric, oceanic and sea ice properties over an annual cycle to better understand the evolution of the upper-ocean stratification process in one of the fastest changing regions of the Arctic Ocean. They were deployed in two different configurations (see Table 1).

(i) Three clusters of three autonomous buoys (an ITP[1], AOFB[2] and WIMBO[3]) were co-located on three separate floes: Cluster 1 (C1), Cluster 2 (C2) and Cluster3 (C3). Only the ITP and WIMBO systems were used in this study.

(ii) Two single WIMBO buoys deployed on separate floes: Solo 1(S1) and Solo 2 (S2).

Near daily Synthetic Aperture Radar (SAR) satellite images, centred on each Cluster and Solo site, were obtained in order to provide a broader spatial context to the *in situ*

[1] Ice Tethered Profiler (ITP): Profiles of temperature, salinity and velocity are obtained from a profiler that crawls along a weighted wire suspended from a surface buoy *(15-16)*.
[2] Autonomous Ocean Flux Buoy (AOFB): monitors velocity, temperature, salinity, and the vertical turbulent fluxes of heat, salt, and momentum in the upper-ocean along with vertical profiles of ocean currents.
[3] Weather, waves, Ice Mass Balance, Ocean buoy (WIMBO): monitors metrological parameters including incoming solar radiation, wind speed and direction, air temperature; ice and snow properties via an ice mass balance (IMB) senor string; and upper-ocean properties via a 200 m temperature and salinity chain.

results. Products used included the publicly available Sentinel-1 imagery, as well as specifically targeted high-resolution imagery: RADARSAT-2, COSMO-SkyMed, and TerraSAR-X. OSISAF ice concentration *(17)* was used to monitor the ice conditions on a synoptic-scale

2. Methods

The dates associated with the start of snowmelt (Stage 1) and meltpond drainage (Stage 2) were obtained from the analysis of near-daily SAR imagery that was targeted at the Clusters and Solo platforms. The identification of these two stages is made possible because SAR image intensity is attenuated as the scattering surface (either snow or ice) becomes wet (Dierking, 2013). When the snow on the ice surface melts, its appearance in a SAR image darkens due to reduced backscatter, and then when the meltponds drain, it brightens again due to enhanced backscatter (See supplementary Fig. S1).

To identify the start of basal melt we identified, within each IMB record, the first date at which the thickness of the ice bottom had been at least 10 cm less than its winter maximum for three consecutive days. As basal melting is related to the break-up of the ice pack, we also ascertained the date when the OSISAF ice concentration at a site dropped below 90% for at least three consecutive days.

Both the ITPs and WIMBOs observed the temperature and salinity structure of the upper-ocean (0-65 m). On each ITP, (i) a Seabird microCAT located at a fixed-depth of 5 m sampled every 15 minutes, and (ii) the profiling CTD sampled every 3 hours with 1 m vertical resolution. Each of the five WIMBO systems measured air-ice-ocean temperatures through the meteorological sensors, the IMB (every 2 cm), and the 200 m T-Chain. The T-Chain measured upper-ocean temperature (0-65 m) with a

vertical resolution of 0.25 m and salinity at discrete depths (5 m and 25 m). Whilst the IMB sampled hourly, the data from other sensors were obtained every 10 minutes in summer and hourly in winter. All data shown covers the period May 1 to July 31, 2019.

3. Results

The drift tracks of the three clusters (C1, C2 and C3) and the two Solo sites (S1 and S2) can be seen in Fig. 1, and the contrasting behaviour in ice concentration along their tracks in Fig. 2. The northern most clusters (C1 and C2) remained within high concentrations of perennial ice in the northern Beaufort Sea for the entire year. Their drift tracks were virtually identical, with a complete ice cover remaining until the end of June, after which the concentration dipped to around 80% before rising again in autumn. The more southerly cluster (C3) drifted east before turning south, following a similar drift track to S1 and S2. It remained in relatively high ice concentrations until mid-June (>80%), after which it reduced to around 60%, recovered slightly, before melting out completely in September. The two Solo platforms (S1, S2), which were deployed at slightly lower latitudes, also drifted eastwards, before more rapidly moving south. The ice around these systems experienced an early and near-continuous reduction in ice concentration from mid-May, eventually melting completely in late July and August respectively. This discrepancy between the near continuous perennial ice-cover around clusters C1 and C2 (a proxy for the traditional Arctic system), and the seasonal ice surrounding C3, S1 and S2 (a proxy for a future seasonal Arctic system) provides an exceptional opportunity to investigate the evolution and impact of melt within these distinct systems.

When considering the development of the sea ice melt cycle we must determine the relative timings of (a) snowmelt, (b) drainage of meltpond (c) pack break-up and (d)

122 basal melt at each site. The dates of each of these are displayed by markers within
123 Figures 2, 4 and 5, and are summarised along with the initial snow and ice conditions
124 in Table 1. All deployment sites had a similar thickness of snow, between 0.15 -0.22
125 m, and an ice thickness of around 1 m, except C3 which had a thickness of over 2 m.

126 Our analysis suggests uniformity in the timing of snowmelt and meltpond drainage
127 throughout the range of latitudes of this study (~70^{o}N to 80^{o}N); snowmelt in mid-to-
128 late June and meltpond drainage in early July. There is however considerable
129 divergence in the timing of basal melt. For the southernmost systems S1 and S2 basal
130 melting started in mid-June, for C3 which was slightly further north it was late June,
131 and the end of July for the northern most C2. Basal melt for C1 could not be
132 determined as the co-deployed WIMBO stopped transmitting in mid-April, but is
133 expected to be like C2. This latitudinal component to the start of basal melt is also
134 apparent in the reduction in sea ice concentration (Fig. 2 and Table 1). Taken together
135 we find that the seasonal ice zone (C3, S1, S2) experiences an early and continuous
136 reduction in sea ice concentration combined with an early start to basal melting,
137 whilst the perennial ice zone (C1, C2) sees a delay in the reduction in ice
138 concentration and a deferred start to basal-melting, in this case more than a month
139 later. This variation in timing is consistent with our knowledge of the impact of the
140 ice-albedo feedback mechanism.

141 Fig. 3 shows the contrasting evolution in cartoon form. Differences between the two
142 regimes are driven by the availability of open water to absorb downwelling solar
143 radiation. It is important to point out that contrasts are not the result of more solar
144 radiation being present at the surface at lower latitudes - quite the reverse, as
145 radiometer measurements from the WIMBO systems showed the northern sites have
146 greater surface insolation (+45 W/m^{2}) than the southern sites (attributed to less

147 cloudiness at higher ice concentration sites). Nor are air temperatures significantly
148 different between the two cases (0.4^{o}C); see supplementary Fig. S2.

149 **3.1. Consequences for the ocean**

150 Given the stark contrasts between the melt processes within the seasonal and
151 perennial ice zones, we can expect the consequences for the upper-ocean to be
152 similarly varied. Here we interpret changes to the ocean mixed layer that is directly in
153 contact with the sea ice in May – July, and during these months it is isolated by strong
154 stratification from the (geographically variable) water masses below. By focusing on
155 the evolution of oceanic properties and the timings of key melt-events at each site, we
156 can better understand how different melt processes influence upper-ocean properties.

157 Fig. 4 shows time/depth evolution of the temperature and salinity structure at a high
158 latitude perennial and the lower latitude seasonal zones, as monitored by sensors on
159 the WIMBOs and ITPs for May through July. As no ITPs were deployed at the Solo
160 sites, we used C3 to represent the seasonal melt cycle and C2 to represent the
161 traditional melt cycle. In addition, Fig. 5 shows the deviation of temperature and
162 salinity from their May 1 values over the subsequent three months, along with the
163 deviation of temperature (T) from its freezing point (T_f) at 5 m depth over the same
164 period, for all Clusters and Solo sites. May 1 was chosen because on this date all sites
165 had a continuous ice cover (see Fig. 2), air temperatures were well below freezing,
166 and there was no evidence melt processes had begun.

167 Though the two northern clusters (C1 and C2) were separated by around 100 km the
168 evolution of upper-ocean properties were similar. For the most of May and June the
169 water temperature remained near T_f, but after snowmelt and subsequent meltpond
170 drainage events we see a slight freshening and warming of the upper-ocean. This

171 steady change in salinity and temperature continued after bottom melt started at the
172 end of July. Overall, we see a 0.2^{o}C rise in temperature and a reduction in salinity of
173 less than 0.5 between May and July. The traditional melt process can be described as
174 having a slight, but relatively consistent, impact on the upper-ocean.

175 At lower latitude sites (S1 and S2) we find the changes in temperature and salinity
176 more pronounced and varied. The combination of melt processes with the influence of
177 other water masses, such as shelf-waters, during their southward drift makes
178 interpretation more complex, and for this reason we include the deviation from
179 freezing point ($T-T_f$) in Fig. 5. The Solo sites were deployed very close to each other,
180 and took similar southerly trajectories, albeit with S1 drifting south of S2. The first
181 striking difference with the northerly clusters is the early start and speed to the
182 warming of the upper-ocean. Between mid-May and the start of snowmelt in mid-
183 June there was an increase in temperature of more than 0.5^{o}C above its freezing point,
184 more than double that seen by the northerly clusters over the entire three months. As
185 the change in temperature was combined with almost no change in salinity, it suggests
186 the influence of solar warming through lead openings. This assumption is
187 corroborated by the reduction in ice concentration which first dropped below 90% in
188 mid-May, and reduced to around 75% by mid-June (Fig. 2).

189 Cluster C3 was located between the northerly clusters and the southerly Solo sites,
190 and its easterly deployment meant that its subsequent drift passed close to the
191 Canadian shelf, and so potentially influenced by shelf-waters. The freshening without
192 deviation from the freezing point that began in mid-May is suggestive of drifting into
193 a region with slightly fresher water properties. Around the start of June there is an
194 increase in temperature above its freezing point of about 0.15^{o}C, before snowmelt was
195 initiated in mid-June. This is consistent with the ice concentration around C3

196 dropping to below 90% at the end of May, again suggesting solar radiation entering
197 the water column through leads. Shortly afterwards basal melt starts (23 June), and
198 the salinity begins to reduce quickly, but the deviation from freezing point
199 temperature remains steady at about 0.15^{o}C. However, the most significant change in
200 temperature coincides with the start of meltpond drainage (4 July), which sees patches
201 of relatively high temperature (1.5^{o}C above T_f) water reaching down to almost 20m
202 depth (see Fig. 4), similar events were seen in S1 and S2. These warm patches could
203 represent local drainage plumes rapidly mixed into the upper 10s of meters of the
204 ocean, or more likely indicate that the C3 platforms drifted though several melt-water
205 plumes that previously entered the ocean from non-local points. In situ measurements
206 of the temperature of water with meltponds suggest it can warm above 0^{o}C *(18)*. Note
207 that the ice thickness at the C3 site went to zero on August 2, which indicates that the
208 floe either melted or broke up.

209 **4. Discussion**

210 Our results suggest the high latitude regions of the Arctic are still representative of
211 perennial ice cover, where surface melt dominates over basal melt, and melting
212 follows the traditional regimented and distinct cycle of *Snowmelt—Pond*
213 *formation/drainage—Basal melt*. The lower latitudes, on the other hand, represent a
214 seasonal ice regime with a reordered melt cycle in which basal melt occurs
215 significantly earlier in the season, in our case almost coincident with snowmelt. We
216 anticipate that the continued early retreat of Arctic ice will further emphasize the
217 importance of basal melt, and will favour a seasonal melt cycle that follows the path
218 of *Basal melt—Snowmelt—Pond formation/drainage*.

219 Which of these two melt cycles dominate appears to be predicated on its ice
220 concentration history. Our data suggests that the early availability of low-albedo

221 open-water is the major factor in warming the upper-ocean and initiating basal melt.
222 This assumption is supported by Kashiwase et al., *(19)* who suggested that the albedo
223 mismatch between ice and water could be a major factor that enhances summer sea
224 ice retreat, caused by early-season divergent motion. An early break up and
225 divergence of the ice pack will favour a seasonal melt cycle, whereas a late season
226 divergence of the pack will result in a more traditional melt cycle.

227 Under the traditional melt progression, the impact of surface and basal melt on the
228 upper-ocean is modest and occurs over several months, which gives longer to slowly
229 mix this freshwater downwards within the surface layer. Intriguingly, in our study the
230 drainage of meltponds had a much smaller influence on the upper-ocean structure at
231 the high latitude sites, despite all Clusters and Solo platforms being surrounded by a
232 similar snow cover (see Table 1). The reason for this reduced effect could be related
233 to the mechanisms controlling the way meltwater flows through the sea ice. It has
234 been suggested by Polashenski et al., *(10)* that the pathways through the sea ice may
235 be plugged by the refreezing of meltwater, and that this process is highly dependent
236 on ice temperature, salinity, and the initial pore size. The median ice temperature
237 when the meltponds drained on 3 July for northern site C2 and southern site S2 was -
238 1.29^{o}C (±0.02 ^{o}C) and -0.87^{o}C (±0.07 ^{o}C) respectively. Thus, with colder ice it is
239 possible that plugging is more prevalent within the high-latitude regions, limiting the
240 upper-ocean response. A secondary effect that may introduce more meltwater to the
241 southern sites is the fractured nature of the sea ice. When snow melts the resultant
242 meltwater spreads horizontally across the surface of the sea ice until it reaches the
243 edge of a floe, where it cascades into the ocean. This process is not as prevalent in
244 regions of higher ice concentration as the floes are bigger meaning the area-to-

perimeter ratio of the floes is considerably larger, thus a higher volume of meltwater will be retained on the floe.

Under a seasonal melt cycle, the timing between the surface and basal melt processes occurs earlier and is considerably narrowed. This allows for substantially more heat (through solar input and meltpond drainage) and freshwater (through basal melt and meltpond drainage) to enter the upper-ocean earlier in the season, and over a condensed period. The contrast between regions of perennial and seasonal ice becomes more pronounced when comparing basal melt rates. Between May and July C2 experiences and average melt rate of a millimetre a day (1.1 mm/day) whilst C3 experiences over the same period almost a centimetre a day (9.7 mm/day), see Fig.4 for location of ice bottom. Furthermore, regions of moderate ice concentration, like C3, will have more efficient coupling between the atmosphere and ocean, thus increasing the transfer of momentum into the upper-ocean and enhancing turbulent mixing *(20)*.

A further impact of a change in the timing and sequence of the melt cycle will be on the under-ice light field. Snow has a very high light-extinction coefficient, up to 40 m^{-1} compared with the sea ice of around 1 m^{-1} (*21-22*). Therefore, as the snow melts the intensity of the under-ice light field increases, which is a major factor for photosynthesis by phytoplankton and ice algae (*23*). *In situ* measurements have shown that rapid snow melting events may result in doubling the amount of solar irradiance under the ice (*24*), but it is only when significant areas of open-water are present, later in the season, that the upper-ocean light field will substantially increase on a large scale. This suggests that under the traditional melt cycle the upper-ocean light field will provide a gradual increase as the season advances. The seasonal melt cycle however, will allow more light to directly enter the water column much early in the

season, because of the break-up and divergence of the pack. Importantly, under that seasonal scenario the reduction in ice concentration occurs before the snow has melted, thus the under-ice light field will still diminished. How the large mismatch in light intensity between open-water regions and under-ice regions influence development of phytoplankton and algae in the Arctic is not clear. This situation is more akin to the seasonal retreat of Antarctic sea ice.

5. Conclusion/Summary

Whilst many of the processes mentioned have been previously studied, it is only by using autonomous air-ice-ocean observations across a latitudinal range, with targeted satellite imagery, that we can provide this comprehensive overview of Arctic melt processes. Together they provide a powerful tool to demonstrate the previously unseen paradigm shift that is taking place in the melt sequence of Arctic sea ice that is summarised by Fig. 3, thereby ensuring basal melt dominates ice loss in this 'new Arctic' analogue.

The reorganisation of sea ice melt processes represents a fundamental change in the Arctic melt regime, one that substantially enhances basal melt and influences the timing and the nature of the evolution of the upper-ocean properties and the under-ice light field. These processes play a crucial role in regulating algal growth and phytoplankton blooms, and hence the transfer of energy and matter to higher trophic levels (*25*). A pan-Arctic shift towards a seasonal melt cycle has the potential to induce a mismatch between the coordination of algal growth, phytoplankton blooms, and zooplankton production, thus disrupting ecosystem dynamics at all trophic levels.

Acknowledgments: This work was supported by an Office of Naval Research (ONR) Departmental Research Initiative called Stratified Ocean Dynamics in the Arctic (SODA), and the work presented here is supported by multiple ONR grants. We would like to acknowledge contributions from all members of the SODA team, and are grateful to captain, officers and crew of the *USCGC Healy*.

Author contributions: JW conceived the idea behind the study, JH, JDL, HG, LR prepared the SAR images, ITP data prepared by SC, WIMBO data by JW, MD and LV. All authors contributed to methodology, analysis, and the writing and reviewing of the manuscript.

Competing interests: Authors declare no competing interests.

Data and materials availability: All data, code, and materials used in the analysis is available to any researcher for purposes of reproducing or extending the analysis.

References:

1. Meier, Walt. N., Greta K. Hovelsrud, Bob E.H. van Oort, Jeffrey R. Key, Kit M. Kovacs, Christine Michel, Christian Haas, Mats A. Granskog, Sebastian Gerland, Donald K. Perovich, Alexander Makshtas and James D. Reist, Arctic sea ice in transformation: A review of recent observed changes and impacts on biology and human activity, *Rev. Geophys*., 52, 185– 217 (2014).

2. Lindsay, R. and Schweiger, A.: Arctic sea ice thickness loss determined using subsurface, aircraft, and satellite observations, *The Cryosphere*, 9, 269–283, (2015).

3. Comiso, J. C. Large decadal decline of the Arctic multiyear ice cover. *Journal of Climate*, *25*(4), 1176-1193 (2012).

4. Spreen, G., Kwok, R., and Menemenlis, D. Trends in Arctic sea ice drift and role of wind forcing: 1992–2009, *Geophys. Res. Lett.,* 38, L19501, (2011).

5. Strong, C., and Rigor, I. G., Arctic marginal ice zone trending wider in summer and narrower in winter, *Geophys. Res. Lett.,* 40, 4864– 4868, (2013).

6. Lebrun, M., Vancoppenolle, M., Madec, G., and Massonnet, F. Arctic sea-ice-free season projected to extend into autumn, *The Cryosphere*, 13, 79–96 (2019).

7. Perovich, D. K. et al. Increasing solar heating of the Arctic Ocean and adjacent seas, 1979–2005: Attribution and role in the ice-albedo feedback. *Geophys. Res. Lett.* 34, L19505 (2007).

8. Perovich, D. K. & Polashenski, C. Albedo evolution of seasonal Arctic sea ice. *Geophys. Res. Lett*. 39, L08501 (2012).

9. Pegau, W. and C. Paulson The albedo of Arctic leads in summer, *Ann. Glaciol*., 33, 221-224 (2001).

10. Polashenski, C., Perovich, D., and Courville, Z. The mechanisms of sea ice melt pond formation and evolution, *J. Geophys. Res*., 117, C01001, (2012).

11. Maykut, G. A. & Perovich, D. K. The role of shortwave radiation in the summer decay of a sea ice cover. *J. Geophys. Res. Oc*eans 92, 7032–7044 (1987).

12. Maykut, G. A. & Untersteiner, N. Some results from a time-dependent thermodynamic model of sea ice. *J. Geophys. Res*. 76, 1550–1575 (1971).

13. Carmack, E., Polyakov, I., Padman, L., Fer, I., Hunke, E., Hutchings, J., Jackson, J., Kelley, D., Kwok, R., Layton, C., Melling, H., Perovich, D., Persson, O., Ruddick, B., Timmermans, M.-L., Toole, J., Ross, T., Vavrus, S., & Winsor, P. Toward quantifying the increasing role of oceanic heat in sea ice loss in the new Arctic. *Bulletin of the American Meteorological Society*, 96(12), 2079–2105 (2015).

14. Gallaher, S. G., Stanton, T. P., Shaw, W. J., Cole, S. T., Toole, J. M., Wilkinson, J. P., Maksym, T., and Hwang, B. Evolution of a Canada Basin ice-ocean boundary layer and mixed layer across a developing thermodynamically forced marginal ice zone, *J. Geophys. Res. Oceans*, 121, 6223– 6250 (2016).

15. Toole, J. M., R. A. Krishfield, M.-L. Timmermans, and A. Proshutinsky The Ice-Tethered Profiler: Argo of the Arctic, *Oceanogr*., 24, 126-135, (2011).

16. Cole, S.T., F.T. Thwaites, R.A. Krishfield, and J.M. Toole, Processing of Velocity Observations from Ice-Tethered Profilers. *Proceedings Oceans 2015 MTS/IEEE*, Washington, D.C. Oct 19-22 (2015).

17. Tonboe, R., Lavelle, J., Pfeiffer, R., and Howe, E. Product User Manual for OSISAF Global Sea Ice Concentration, available at: http://osisaf.met.no/docs/osisaf_cdop3_ss2_pum_ice-conc_v1p6.pdf (2016).

18. Kashiwase, H., Ohshima, K.I., Nihashi, S. et al. Evidence for ice-ocean albedo feedback in the Arctic Ocean shifting to a seasonal ice zone. *Sci Rep* 7, 8170 (2017).

19. Martin, T., Steele, M., & Zhang, J. Seasonality and long-term trend of Arctic Ocean surface stress in a model. *Journal of Geophysical Research*, Oceans, 119, 1723–1738. (2014).

20. Perovich, D. K. and A.J. Gow A quantitative description of sea ice inclusions, *J. Geophys. Res*., 101(C8), 18327– 18343, (1996).

21. Light, B., D.K. Perovich, M.A. Webster, C. Polashenski and R. Dadic Optical properties of melting first-year Arctic sea ice, *J. Geophys. Res. Oceans*, 120, 7657–7675, (2015).

22. Arrigo, Kevin R., Perovich, Donald K., Pickart, Robert S., Brown, Zachary W., van Dijken, Gert L., Lowry, Kate E., Mills, Matthew M., Palmer, Molly A., Balch, William M., Bahr, Frank, Bates, Nicholas R., Benitez-Nelson, Claudia, Bowler, Bruce, Brownlee, Emily, Ehn, Jens K., Frey, Karen E., Garley, Rebecca, Laney, Samuel R., Lubelczyk, Laura, Mathis, Jeremy, Matsuoka, Atsushi, Mitchell, B. Greg, Moore, G.W.K., Ortega-Retuerta, Eva, Pal, Sharmila, Polashenski, Chris M., Reynolds, Rick A., Schieber, Brian, Sosik, Heidi M., Stephens, Michael and Swift, James H. Massive phytoplankton blooms under Arctic sea ice. *Science*, 336 (6087), p1408 (2012).

23. Lei, R., Zhang, Z., Matero, I., Cheng, B., Li, Q., & Huang, W. Reflection and transmission of irradiance by snow and sea ice in the central Arctic Ocean in summer 2010. *Polar Research*, *31*(1), 17325 (2012).

24. Wassmann, P., and M. Reigstad. Future Arctic Ocean seasonal ice zones and implications for pelagic-benthic coupling. *Oceanography* 24(3):220–231 (2011).

Platform identifier (listed from north to south at deployment)	Co-deployed Platform/s	Initial snow and sea ice thickness (m)	Date ice concentration dropped to below 90% from OSISAF data	Date basal melt started, as seen by IMB	Date snowmelt started as seen by SAR imagery	Date meltpond drainage started as seen by SAR imagery
Cluster 2 (perennial ice cover)	**WIMBO4, ITP104, AOFB42**	Snow: 0.17 m Ice: 1.44 m (80.53°N, 136.64°W)	**29 June 2019** (81.55°N 126.03°W)	**28 July 2019** (81.77°N 128.51°W)	**15 June 2019** (81.83°N 125.67°W)	**3 July 2109** (81.49°N 126.42°W)
Cluster 1 (perennial ice cover)	**WIMBO3, ITP105, AOFB41**	Snow: 0.22 Ice: 1.16 m (80.12°N, 141.22° W)	**03 July 2019** (80.94°N 130.41°W)	N/A (WB03 lost early)	**19 June 2019** (81.31°N 130.26°W)	**26 June–3 July 2019*** (80.94°N 130.41°W)
Cluster 3 (seasonal ice cover)	**WIMBO2, ITP103, AOFB40**	Snow: 0.16 m Ice: 2.35 m (78.90°N 134.90°W)	**30 May 2019** (78.28°N 126.90°W)	**23 June 2019** (77.37°N 127.15°W)	**15 June 2019** (77.93°N 127.86°W)	**28 June–4 July 2019*** (76.95°N 129.97°W)
Solo 1 (seasonal ice cover)	**WIMBO1**	Snow: 0.15 m Ice: 0.93 m (78.11° N, 138.12° W)	**19 May 2019** (74.70°N 129.34°W)	**14 June 2019** (73.65°N 131.97°W)	**24 May-13 June 2019*** (73.81°N 132.20°W)	**26 June-3 July 2019*** (71.32°N 130.26°W)
Solo 2 (seasonal ice cover)	**WIMBO6**	Snow: 0.17 m Ice: 0.92 m (77.92°N, 138.98°W)	**14 May 2019** (76.47°N 129.81°W)	**15 June 2019** (76.00°N 130.92°W)	N/A (SAR not available)	N/A (SAR not available)

Table 1. Table identifying the buoys associated with each cluster and solo platform (working from high latitude to low latitude), the ice conditions and location of deployment, the dates and location associated with the reduction of ice concentration below 90%, the start of basal melt (identified from IMB data), the start of snowmelt (identified from SAR analysis) and the drainage of meltponds (identified from SAR analysis). The timelines associated with these three processes are represented by the colours green (the process happened first), yellow (second), orange (third) and red (forth).

* Daily SAR not available, therefore a range of dates given that covers the gap in SAR data. In these cases, the latest date was used.

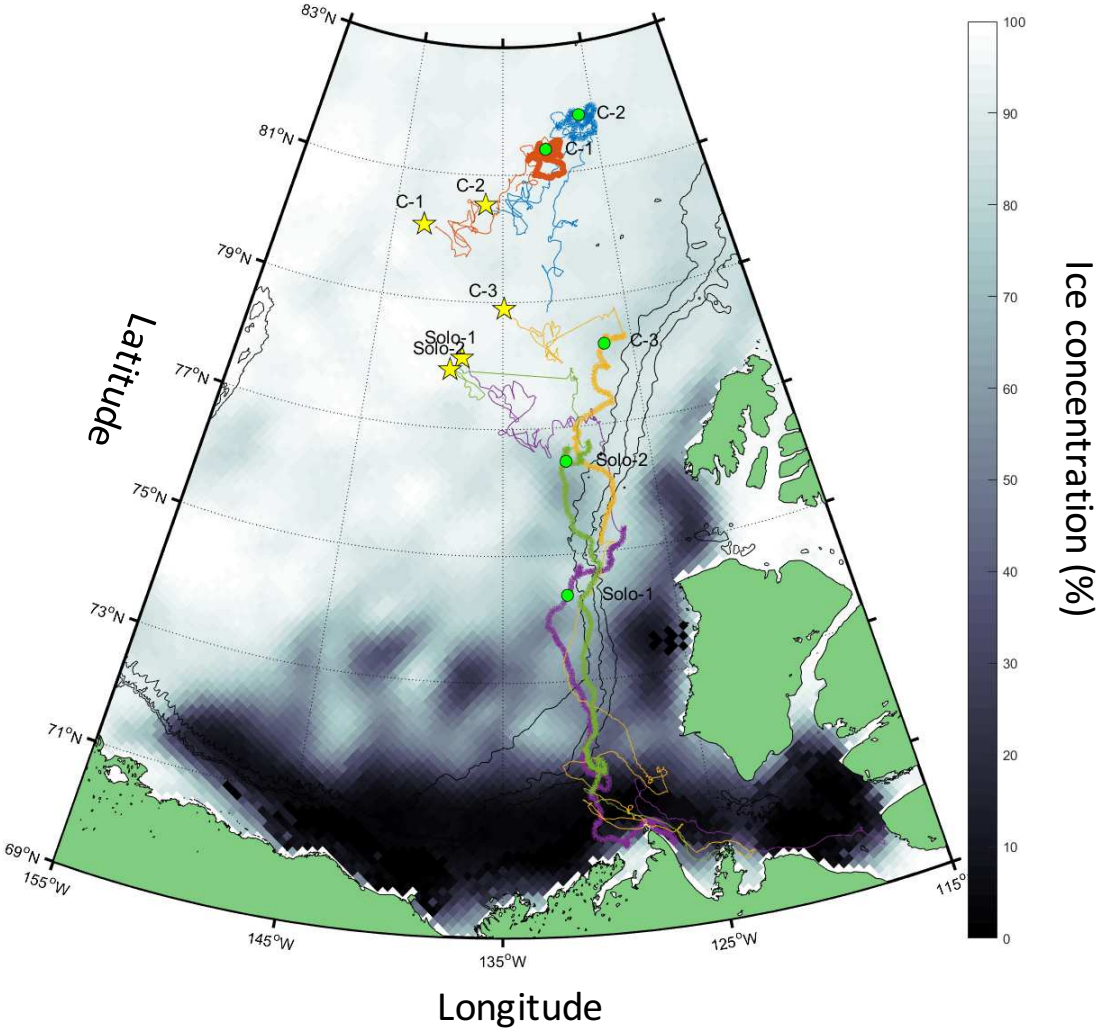

382

383 **Fig. 1.** Drift tracks for Cluster 1 (red), Cluster 2 (blue), Cluster 3 (yellow), Solo1 (purple), Solo 2 (green). The thicker
384 lines represent the drift track from 1 May to 31 July. Notice that Cluster 1 and 2 stay in the north, whilst all the other
385 systems drift southward over time (especially S1 and S2 which are close to the coast by the end of July). The yellow
386 star represents their deployment location, the green circle represents their location on 1 June 2019, the same date at
387 the underling OSISAF ice concentration image (which runs from white or 100% ice concentration through to black
388 0% or open water). The 2000 m, 1000 m, 500m bathymetric contour lines (in black) are also shown.

389

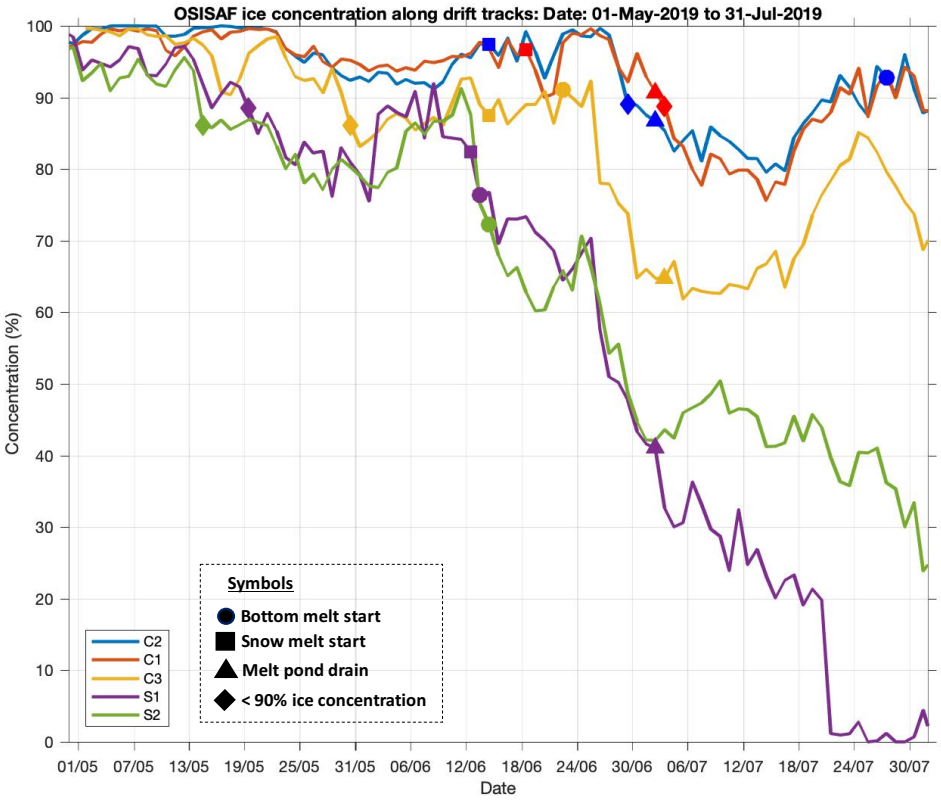

Fig. 2. Graph showing ice concentration against date (from May 1 to July 31, 2019) along the track of each Cluster and Solo platform. Also shown is start of start of the basal melt (circle), snowmelt (square), when the meltponds drained (triangle), and when the ice concentration dropped below 90% for more than three consecutive days (diamond). Notice how the timings of snowmelt and meltpond drainage vertically align across the Clusters and Solo platforms, whilst there is a large separation in time in the ice concentration dropping below 90% and basal melt starting between the northerly clusters (C2 and C1) and the southerly platforms (C3, S1 and S2).

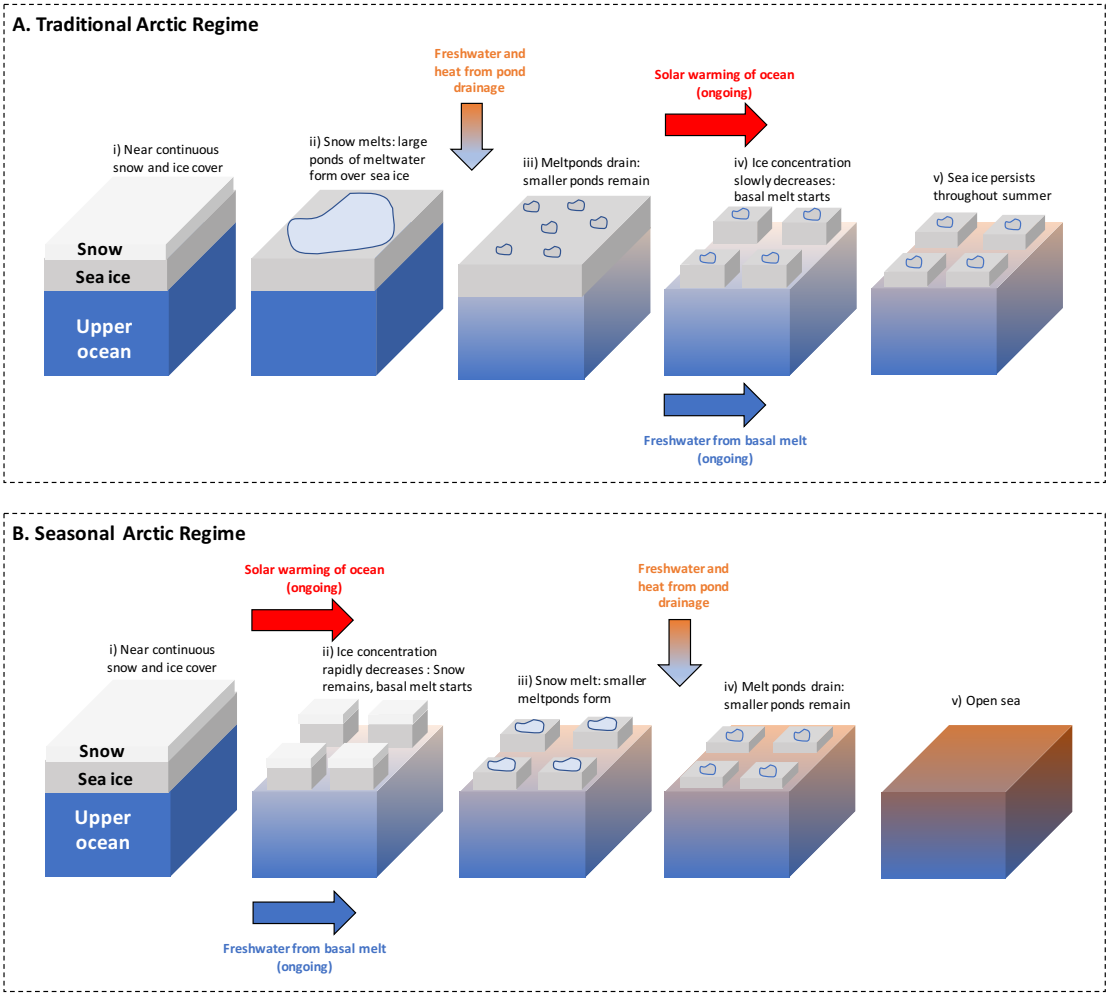

Fig. 3. Schematic representation of the traditional and seasonal melt cycles. Melt season progresses from left to right. Top: traditional *snowmelt—pond formation/drainage —basal melt* cycle that has traditionally existed within a perennial ice dominated Arctic. Bottom: the *basal melt —snowmelt—pond formation/drainage scenario* that may exist within a seasonal ice dominated Arctic.

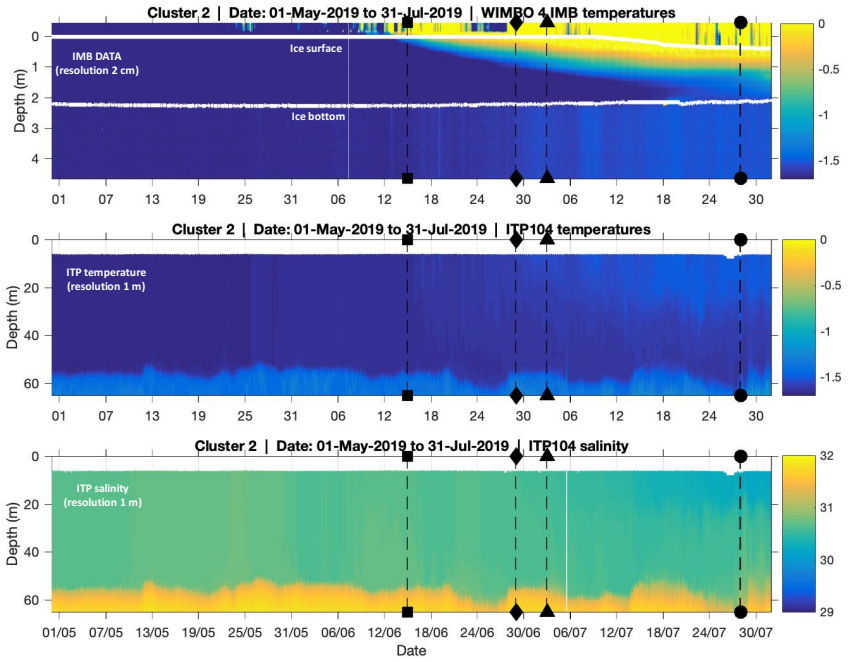

Fig. 4a. Temperature and salinity properties for the northern C2 between May1 and July 31, 2019. Scales are the same as in Fig 4b which shows similar properties for the southern C3. The black dotted lines with symbols identifies when basal melt started (circle), when snowmelt started (square), when the meltponds drained (triangle), and when the ice concentration first dropped below 90% for more than three consecutive days (diamond). Top: Air, snow, sea ice and upper-ocean temperatures from IMB on WIMBO4 (white lines represent the bottom and top of the sea ice); Middle: Upper-ocean temperatures from ITP104 profiler; and Bottom: Upper-ocean salinity from ITP104 profiler

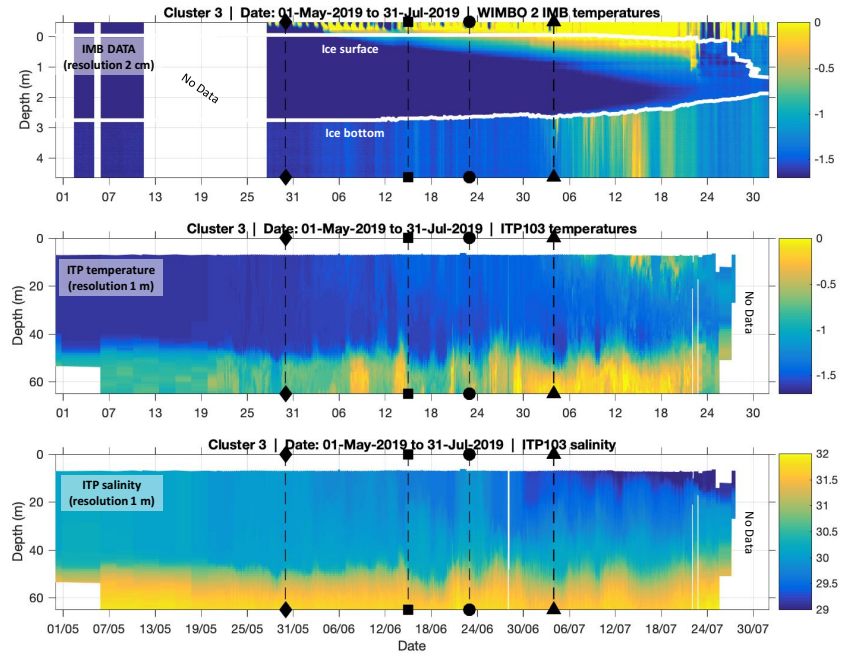

Figure 4b. As above but for the southern **Cluster 3**, but using WIMBO2 and ITP-103 data

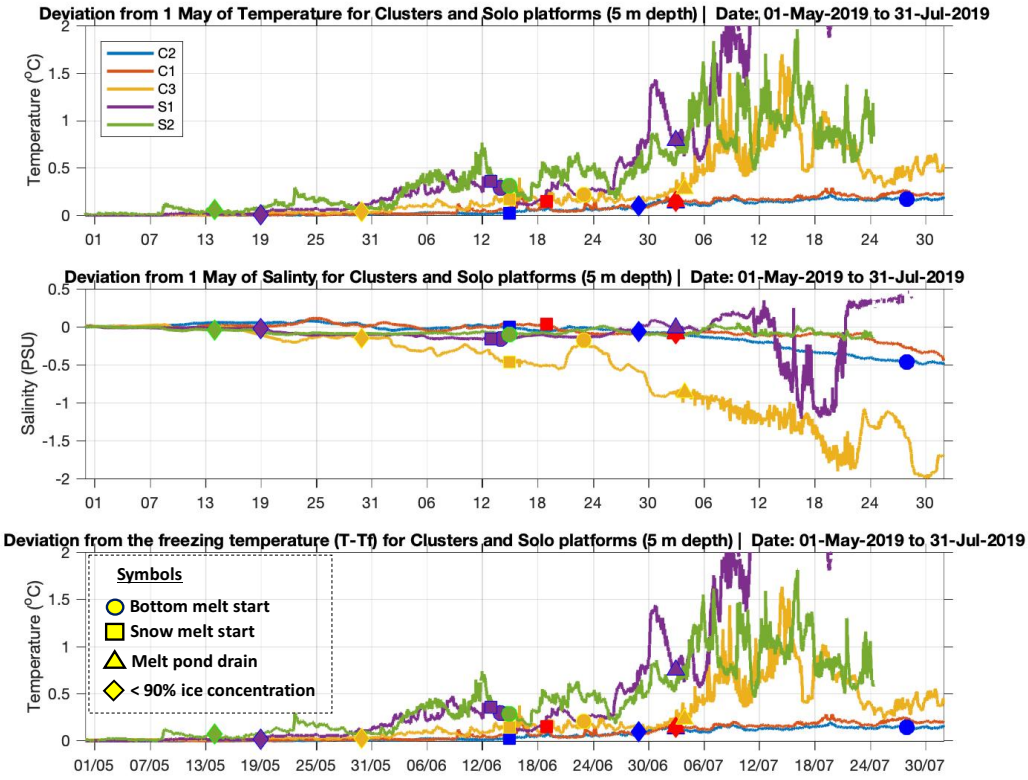

Fig. 5. Deviation of temperature and salinity from their May 1 values over the subsequent three months, along with the deviation of temperature (T) from its freezing point (T_f) at 5 m depth, for all Clusters and Solo sites. Timeline is from May 1 through to 31 July, and the x-axis is limited in temperature to between 0 and 2ºC

Top: Temperature from the Microcat CTD at 5 m depth at C2: ITP104 (blue), C1:ITP103 (orange), and C3:ITP105 (yellow), along with 5 m temperature from S1:WIMBO1 (purple) and S2:WIMBO2 (green): The filled circles, squares, triangles and diamonds identifies when basal melt started, when snowmelt was initiated, when meltponds drained, and when the ice concentration dropped below 90% for more than three consecutive days.

Middle: As above, but for salinity.

Bottom: As above, but for deviation from freezing temperature ($T-T_f$).

Supplementary Materials

Fig. S1.

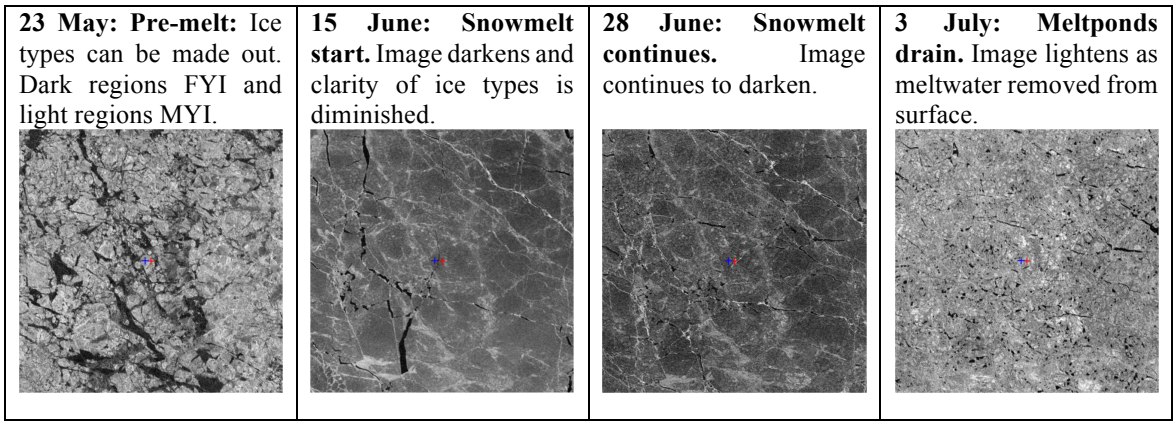

Fig. S1. A 10 x 10 km SAR image showing the ice conditions surrounding Cluster 2. The red cross shows the location of ITP104, and the blue cross shows the location of WIMB04. Working from upper left to bottom right we see the pre-melt conditions through to the first signs of snow melt, to continued melt, and then melt-pond drainage.

436 **Fig. S2.**

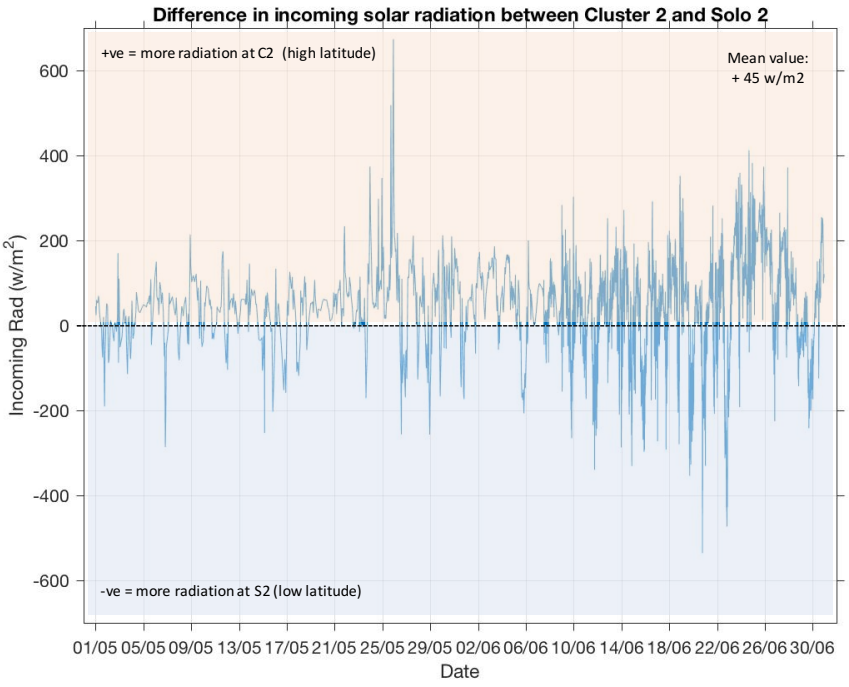

437

438 **Fig. S2a.** Difference between the solar radiation experienced at C2 (high ice concentration) and S2 (low ice
439 concentration). In general, C2 experience 45 w/m^2 more radiation than S2, despite being at a higher latitude.

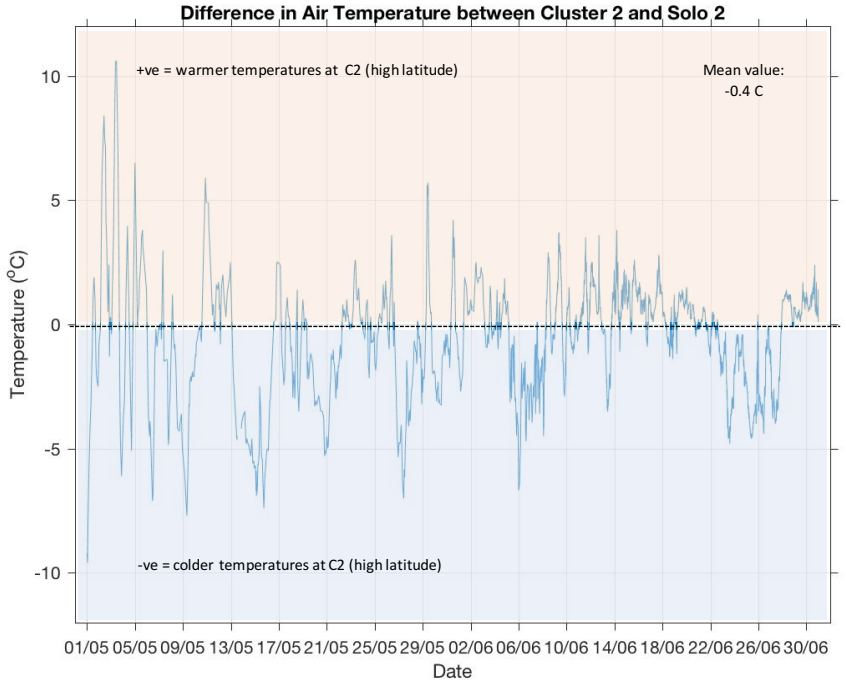

440

441 **Fig. S1a.** Difference between the air temperature experienced the northern C2 (high ice concentration) and that seen
442 by southern platform S2 (low ice concentration). In general, C2 was about 0.4°C colder than the more southerly S2.

Figures

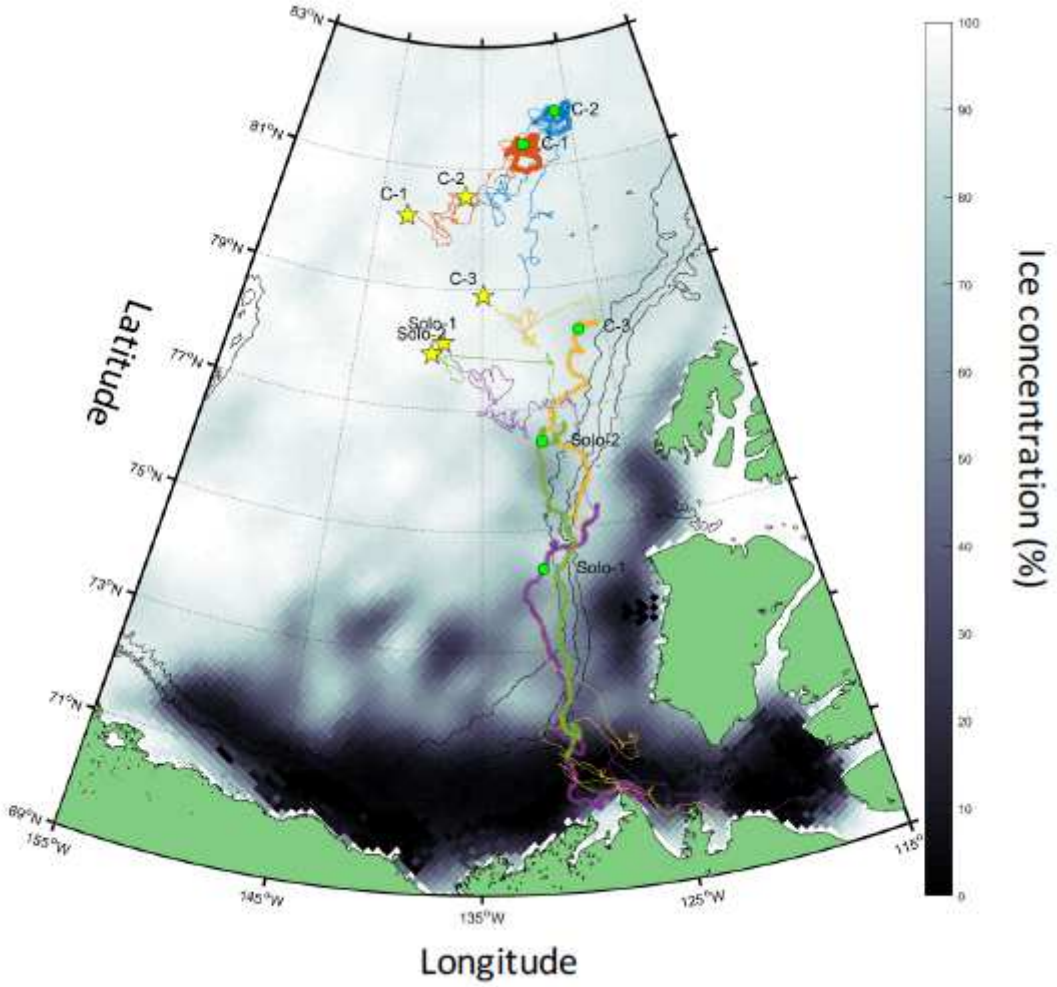

Figure 1

Drift tracks for Cluster 1 (red), Cluster 2 (blue), Cluster 3 (yellow), Solo1 (purple), Solo 2 (green). The thicker lines represent the drift track from 1 May to 31 July. Notice that Cluster 1 and 2 stay in the north, whilst all the other systems drift southward over time (especially S1 and S2 which are close to the coast by the end of July). The yellow star represents their deployment location, the green circle represents their location on 1 June 2019, the same date at the underling OSISAF ice concentration image (which runs from white or 100% ice concentration through to black 0% or open water). The 2000 m, 1000 m, 500m bathymetric contour lines (in black) are also shown.

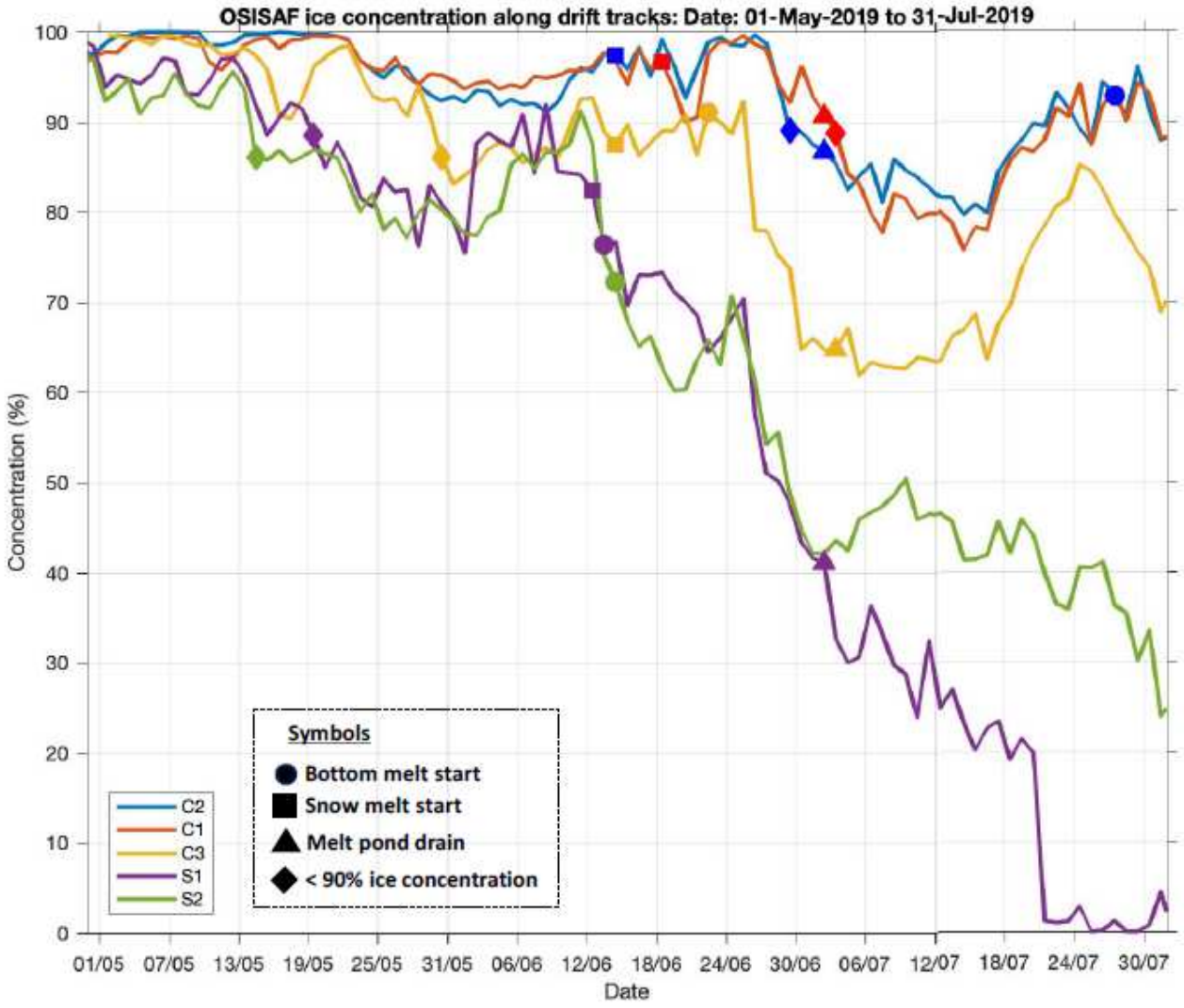

Figure 2

Graph showing ice concentration against date (from May 1 to July 31, 2019) along the track of each Cluster and Solo platform. Also shown is start of start of the basal melt (circle), snowmelt (square), when the meltponds drained (triangle), and when the ice concentration dropped below 90% for more than three consecutive days (diamond). Notice how the timings of snowmelt and meltpond drainage vertically align across the Clusters and Solo platforms, whilst there is a large separation in time in the ice concentration dropping below 90% and basal melt starting between the northerly clusters (C2 and C1) and the southerly platforms (C3, S1 and S2).

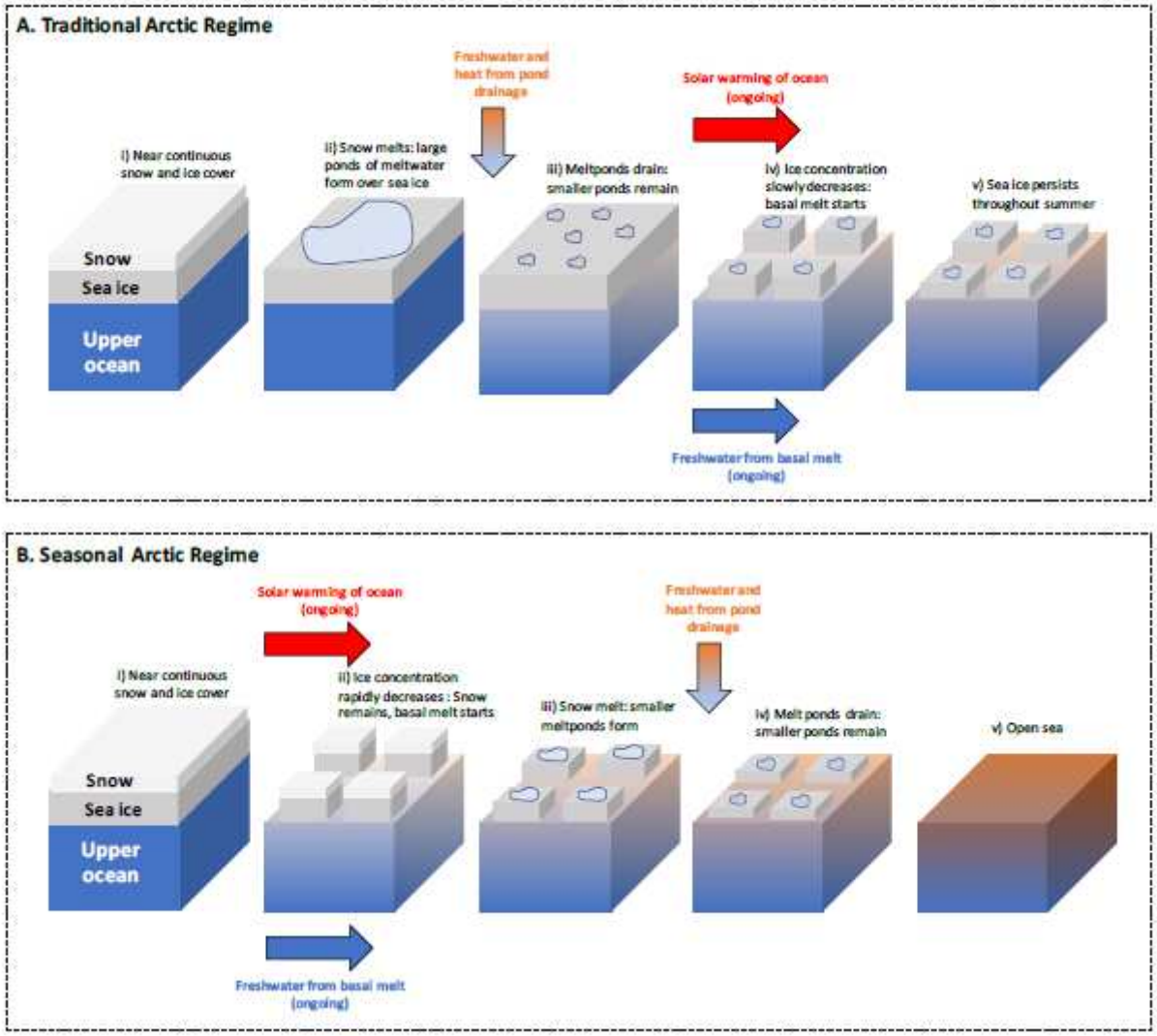

Figure 3

Schematic representation of the traditional and seasonal melt cycles. Melt season progresses from left to right. Top: traditional snowmelt—pond formation/drainage —basal melt cycle that has traditionally existed within a perennial ice dominated Arctic. Bottom: the basal melt —snowmelt—pond formation/drainage scenario that may exist within a seasonal ice dominated Arctic.

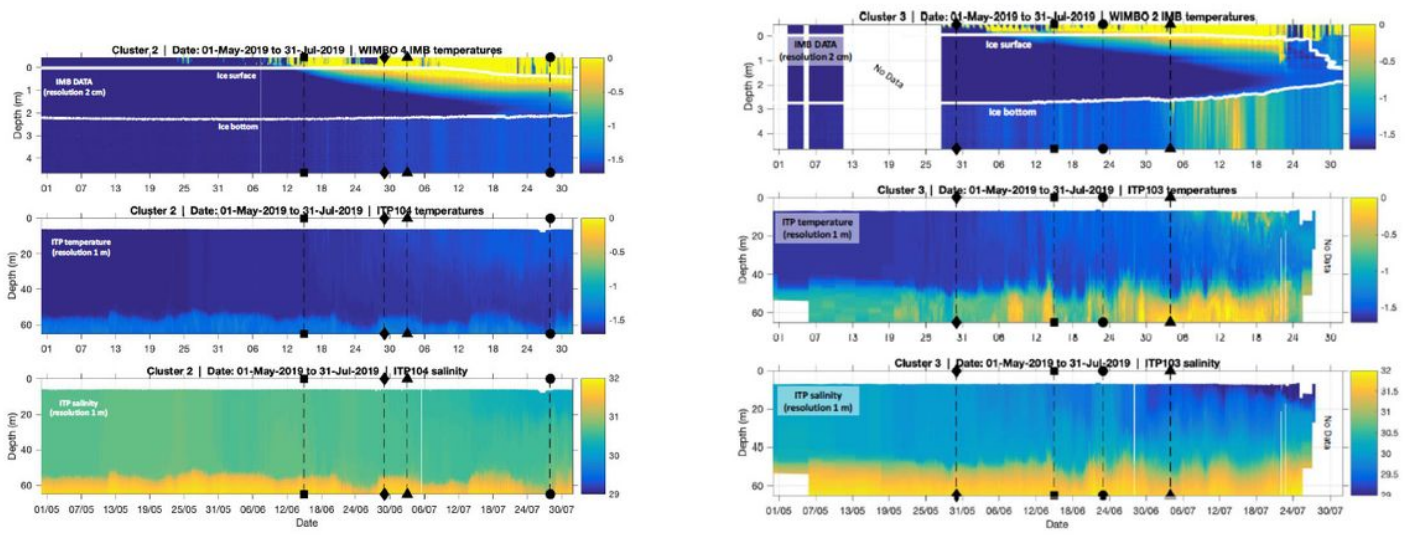

Figure 4

(Left)a. Temperature and salinity properties for the northern C2 between May1 and July 31, 2019. Scales are the same as in Fig 4b which shows similar properties for the southern C3. The black dotted lines with symbols identifies when basal melt started (circle), when snowmelt started (square), when the meltponds drained (triangle), and when the ice concentration first dropped below 90% for more than three consecutive days (diamond). Top: Air, snow, sea ice and upper-ocean temperatures from IMB on WIMBO4 (white lines represent the bottom and top of the sea ice); Middle: Upper-ocean temperatures from ITP104 profiler; and Bottom: Upper-ocean salinity from ITP104 profiler (Right) 4b. As above but for the southern Cluster 3, but using WIMBO2 and ITP-103 data

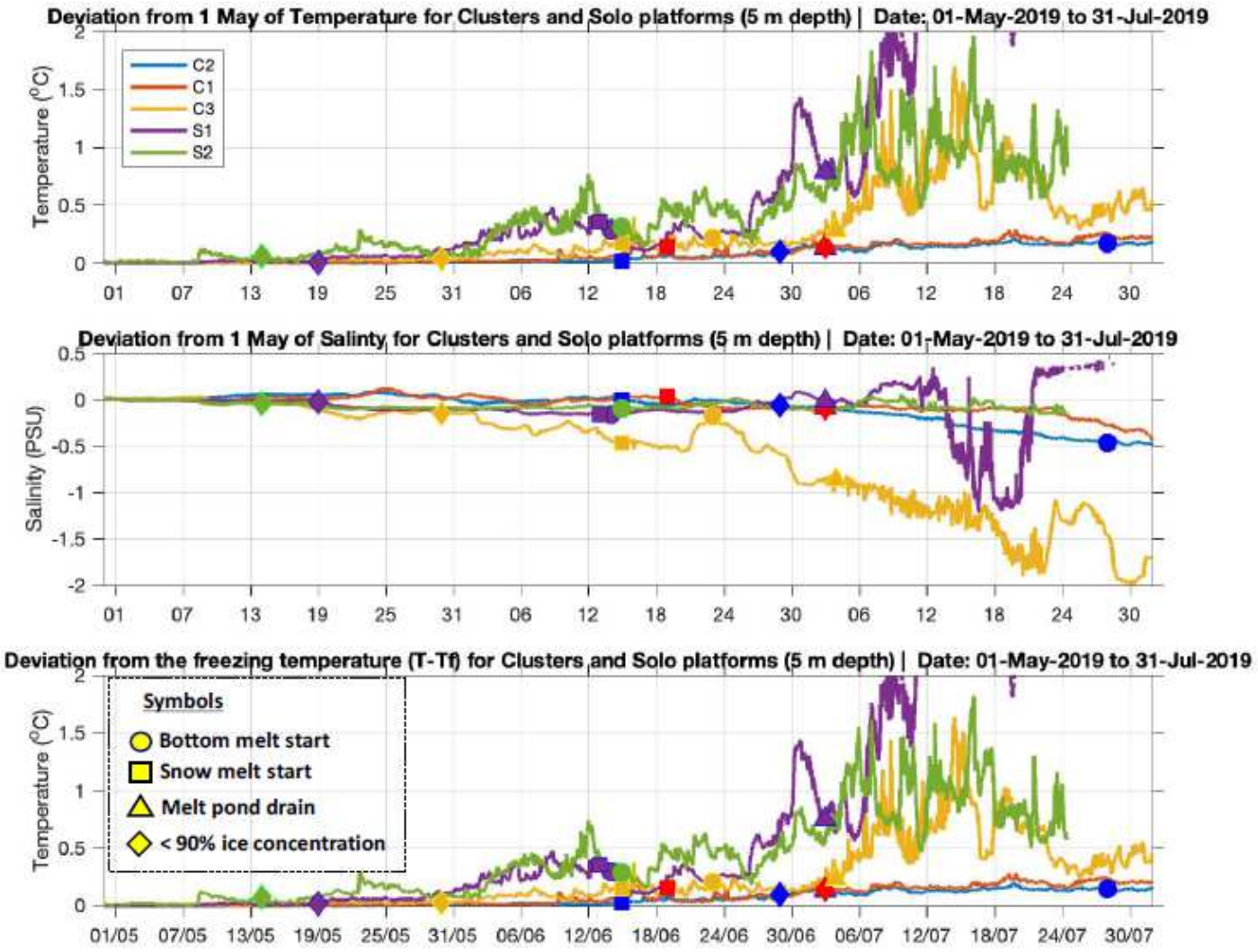

Figure 5

Deviation of temperature and salinity from their May 1 values over the subsequent three months, along with the deviation of temperature (T) from its freezing point (Tf) at 5 m depth, for all Clusters and Solo sites. Timeline is from May 1 through to 31 July, and the x-axis is limited in temperature to between 0 and 2ºC Top: Temperature from the Microcat CTD at 5 m depth at C2: ITP104 (blue), C1:ITP103 (orange), and C3:ITP105 (yellow), along with 5 m temperature from S1:WIMBO1 (purple) and S2:WIMBO2 (green): The filled circles, squares, triangles and diamonds identifies when basal melt started, when snowmelt was initiated, when meltponds drained, and when the ice concentration dropped below 90% for more than three consecutive days. Middle: As above, but for salinity. Bottom: As above, but for deviation from freezing temperature (T-Tf).

Supplementary Files

This is a list of supplementary files associated with this preprint. Click to download.

- FigS1.png
- FigS2final.jpg